Dalton Transactions

ROYAL SOCIETY OF CHEMISTRY

PAPER

View Article Online
View Journal | View Issue

Cite this: *Dalton Trans.*, 2024, **53**, 3880

Carbone stabilized B_2 and B_2^{2+} – isoelectronic analogues to diborabutyne and diborabutatriene†

Jishnu Sai Gopinath, Naseeha Vadakkathodika and Pattiyil Parameswaran *

Received 28th December 2023,
Accepted 22nd January 2024

DOI: 10.1039/d3dt04358d

rsc.li/dalton

It has been reported that various unusual main group compounds can be stabilized by coordinating with ligands. Here, we report the use of carbone ligands in stabilizing diboron in its neutral and dicationic states by computational quantum mechanical calculations. The neutral $[(L_2C)\cdot B_2\cdot(CL_2)]$ (L = CO, NHC, PMe_3, and cAAC) has singlet non-planar cumulenic-type equilibrium geometry where CL_2 groups are almost orthogonal to each other. MO analysis indicates that the $[(L_2C)\cdot B_2\cdot(CL_2)]$ can be considered as formed by the interaction of the B_2 fragment in the $^1\Sigma_g^+$ excited state with two CL_2 ligands having σ- and π-type lone pairs. Accordingly, the π delocalization in the C–B–B–C skeleton consists of two mutually orthogonal allylic anionic-type delocalizations along the C–B–B chain. Since one of the π-delocalized MOs of allylic anionic C–B–B is majorly localized on the carbone carbon atom, the carbone ligands formally act as two-electron ligands. On the other hand, the ground state of $[(L_2C)\cdot B_2\cdot(CL_2)]^{2+}$ shows a singlet planar/pseudo-planar cumulenic geometry when L = NHC and PMe_3. The MO analysis indicates that the C–B–B–C skeleton is similar to that of butatriene, *viz*. one localized B–B π MO, and two delocalized C–B–B–C π MOs, indicating that each carbone acts as a four-electron ligand. Since CO and cAAC are good π-acceptor ligands, $[(L_2C)\cdot B_2\cdot(CL_2)]^{2+}$ ions (L = CO and cAAC) have triplet non-planar cumulenic ground states.

Introduction

The stabilization of diboron in its neutral state and in other oxidation states is challenging for synthetic chemists.[1,2] The diboron in its ground state exists in a $^3\Sigma_g^-$ electronic state having two half π bonds ($1\sigma_g^2 1\sigma_u^2 1\pi_u^1 \pi'_u{}^1$, Scheme 1a), and this was isolated only in an argon matrix.[3] The B_2 unit can accept up to eight electrons if the $1\pi_u$, $1\pi'_u$, $2\sigma_g$, $1\pi_g$ and $1\pi'_g$ orbitals are susceptible to electron acceptance. This is based on the assumption that the energy difference between the $2\sigma_g$ and $1\pi_g$ type orbitals is quite low. On the other hand, the dicationic diboron system ($1\sigma_g^2 1\sigma_u^2 1\pi_u^0 1\pi'_u{}^0 1\pi_g^0 1\pi'_g{}^0$) can accept up to 10 electrons. Many attempts to stabilize the neutral diboron moieties resulted in L_2B_2, L_3B_2, and L_4B_2 types of compounds where L = 2 electron donor ligands (Scheme 1b).

The first ligand-stabilized B_2 was reported by Zhou *et al.* in 2002. They synthesized $B_2(CO)_2$ in an argon matrix at 8 K (Scheme 1b(i)).[4] It was the first report of a triple-bonded diboron complex with a B–B bond length of 1.468 Å. Later, Mavridis *et al.* theoretically explored L_2B_2 compounds where the ligands were CO, CS, N_2, Ar, and Kr.[5] They found out that B_2 acts as an acceptor group, whereas the ligand species serve as donor groups to form donor–acceptor interactions in all compounds. In another case, Li and co-workers detected $[(BO)_2B_2]^-$ in the gas phase using photoelectron spectroscopy.[6] The corresponding dianionic system resembled $[(CO)_2B_2]$ and exhibited a triple bond between the boron atoms (Scheme 1b (ii)). Energy decomposition analysis (EDA) combined with the natural orbitals for chemical valence (NOCV) study of OCBBCO, N_2BBN_2, and $[OBBBBO]^{2-}$ by Frenking *et al.* established the donor–acceptor nature of the L–B bond.[7] The experimental breakthrough of synthesizing an isolable triple-bonded diboron stabilized by Arduengo-type N-heterocyclic carbene (NHC) units was reported in 2012 (Scheme 1b(iii)).[8] Molecular orbital (MO) analysis showed that the two highest occupied orbitals are the orthogonal π orbitals residing in the B_2 moiety.[9,10] The boron–boron bond multiplicity in all the above systems can be considered as three *viz*. one σ bond and two π bonds.

The insertion of the two NHC units into the linear diborene resulted in an NHC-coordinated diborene (Scheme 1b(iv)).[11] Braunschweig *et al.* synthesized cAAC-supported diboron, and their detailed study indicates a diborabutatriene-type bonding pattern.[12] This can be attributed to the better π-accepting nature of the cAAC groups as compared to the Arduengo-type NHC.[13,14] The variation in geometrical patterns in the NHC and cAAC coordinated diboron system indicates that the elec-

Department of Chemistry, National Institute of Technology Calicut, Kozhikode, Kerala, 673601, India. E-mail: param@nitc.ac.in

† Electronic supplementary information (ESI) available. See DOI: https://doi.org/10.1039/d3dt04358d

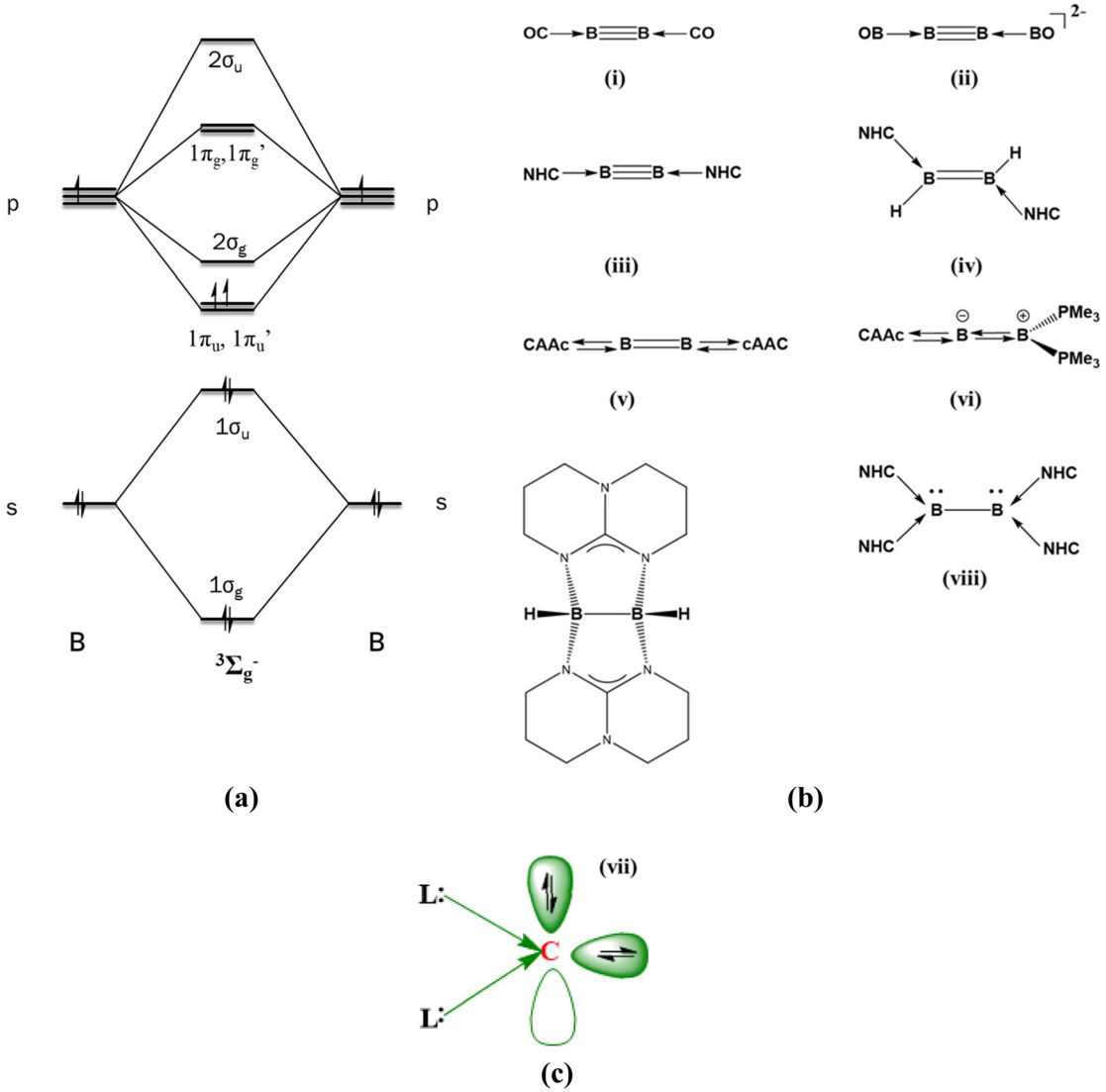

Scheme 1 (a) MO diagram of the ground state of B_2. (b) Various reported ligand-coordinated B_2 molecules. (c) Schematic representation of a bonding picture in CL_2.

tronic structure of the B_2 unit is easily tunable. Kinjo and Braunschweig reported non-planar cumulenic-type diborenes by coordinating one cAAC ligand at one terminal end and phosphene/NHC/cAAC at the other (Scheme 1b(vi)).[15–17] In these cases, the boron–boron bond multiplicity is two with one σ and one π bond. There are also reports of ligand-assisted B_2 molecules with only a boron–boron σ bond. In 2007, Himmel *et al.* reported a guanidine-supported diborane (Scheme 1b (vii)).[18] Recently, a tetrakis NHC-supported diboron was synthesized (Scheme 1b(viii)).[19] This molecule possesses a B–B single bond and a lone pair on each boron. There are also some other studies that feature the stabilization of the B–B bond.[20,21] All the above-mentioned compounds are examples of B_2 units stabilized by two-electron donor ligands, and the number of ligands varies from two to four. The number and nature of the two-electron ligand determines the geometry and bonding patterns of the resultant compounds. Even though B_2 and B_2^{2+} are, in principle, 8/10-electron acceptor groups, stabilizing these species by four-electron donor ligands such as carbones is still elusive.

Carbones (CL_2) are dicoordinate carbon compounds that coordinate to two σ-donor ligands in their ^1D state and retain all their valence electrons as two lone pairs.[22–25] In contrast to the carbenes, which possess a lone pair and a vacant orbital (singlet) or two unpaired electrons (triplet), carbones possess two lone pairs. Therefore, it can act as either a two-electron donor ligand or a four-electron donor ligand. One of the lone pairs is σ type, and the other is π type (Scheme 1c). The first class of synthesized carbones was carbodiphosphorenes, and later carbodicarbenes and other σ-donating ligand-supported CL_2 compounds were also studied.[26–30] CL_2 acting as ligands in transition metal complexes are also widely reported.[31] The carbone-coordinated transition metals are highly active as catalysts in many reactions, such as hydrogenation of olefins, C–C

coupling reactions, hydroamination, *etc*.[32–35] They are also suitable double Lewis donors in stabilizing many species.[36,37] Frenking and Hermann have already theoretically studied the stabilization of isoelectronic main group atoms and ions using carbones as ligands.[38] This study envisaged that carbone can act as a six-electron donor. The bond dissociation energy suggested that carbone coordination stabilizes the main group atoms or ions and compounds more strongly than a two-electron ligand.[39] Note that the phosphorous analogue P[C(NHC^{Me})$_2$]$_2^{3+}$ has already been reported.[40] This shows that four-electron donor carbones can act as better-stabilizing ligands than the typical two-electron ligands. However, no studies have been reported to date using two carbone ligands in stabilizing the main group diatomics. These carbone ligands are expected to stabilize the electron-deficient main group diatomics as they are capable of donating four electrons, *viz*. two electrons in the σ-plane and two electrons in the π-plane.

Here, we report the geometric and bonding pattern of the molecules obtained by coordinating two carbone groups with B_2 and B_2^{2+} using computational quantum mechanical calculation at the M06/def2-TZVPP//BP86/def2-TZVPP level of theory. The studies show that the nature of the carbones and the oxidation state of B_2 determines the geometry and bonding pattern. We expect that this study will trigger experimentalists to use carbone ligands in stabilizing the electron-deficient main group diatomics.

Results and discussion

Structure and bonding analysis of doubly carbone-coordinated diboron

The optimized ground state geometries of [(L$_2$C)·B$_2$·(CL$_2$)] are shown in Fig. 1. **A1–A4** denote neutral [(L$_2$C)·B$_2$·(CL$_2$)] compounds and the numbers **1–4** indicate the type of carbone coordinated to B_2. The number **1** indicates that the carbone coordinated to B_2 is C(CO)$_2$; similarly, numbers **2**, **3** and **4** indicate that the carbone coordinated to B_2 is C(NHC)$_2$, C(PMe$_3$)$_2$ and C(cAAC)$_2$, respectively. The use of T in parentheses indicates the triplet state isomer of the molecule (Fig. S1†). For optimization, the initial geometries considered were the ones with the highest symmetries, *viz*., the non-planar cumulene-type (D_{2d}) structure with the CL$_2$ fragments perpendicular to each other and the planar cumulene-type geometry (D_{2h}) with two coplanar CL$_2$ fragments (Scheme 2). The equilibrium geometries of all the molecules in their singlet and triplet states were calculated (Fig. S1†). All compounds possess a singlet ground state consisting of a linear C–B–B–C skeleton with CL$_2$ fragments close to orthogonal planes. The energy difference between the singlet and triplet states lies within the 1–25 kcal mol^{-1} range, with the energy difference for **A1** (0.9 kcal mol^{-1}) being least and that for **A2** (25 kcal mol^{-1}) being highest. The triplet **A3(T)** is not a stationary point on the potential energy surface, and all attempts to optimize the triplet **A3(T)** lead to the detachment of the PMe$_3$ ligands. The singlet **A4** is more

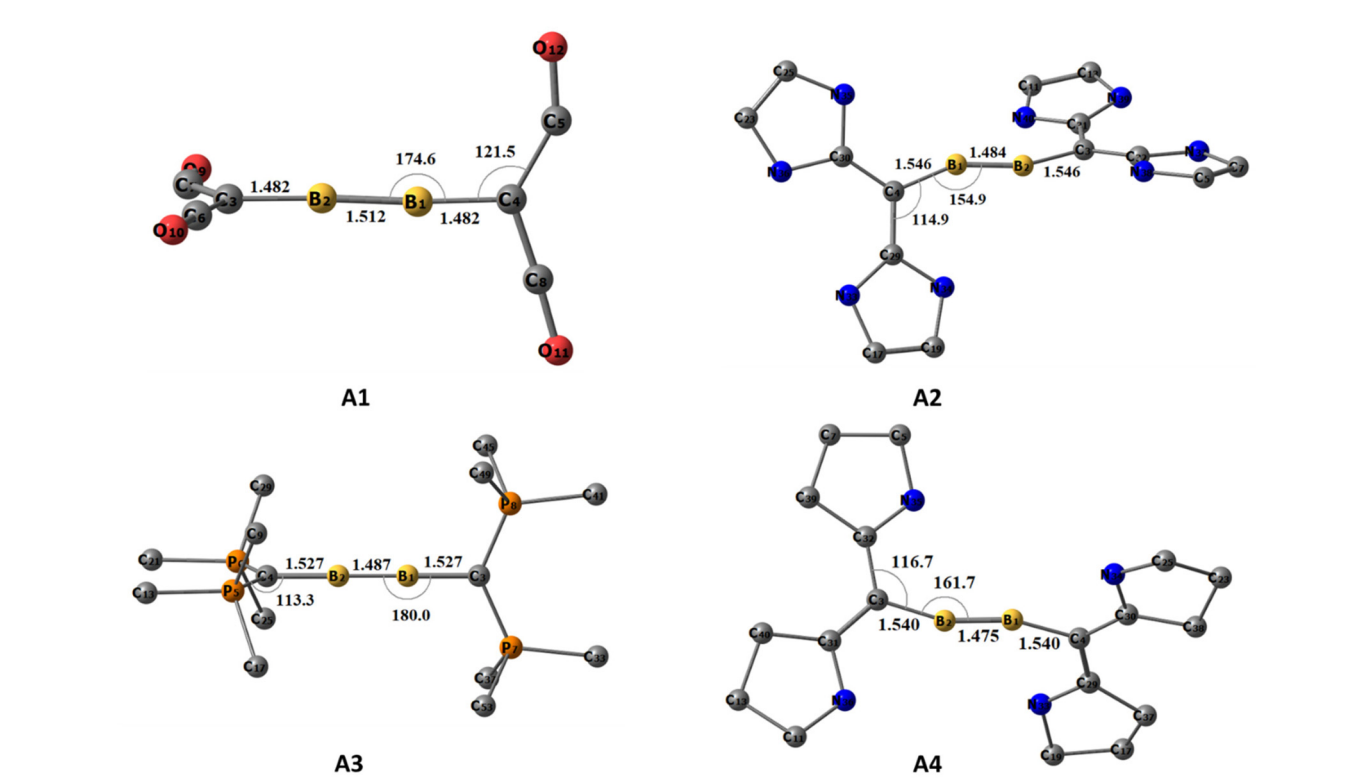

Fig. 1 The equilibrium geometries and the important structural parameters of **A1–A4** at the BP86/def2-TZVPP level of theory. Distances are given in Ångstroms, and angles are given in degrees. Hydrogens are omitted for a better view.

Non-planar cumulene (D_{2d}) Planar cumulene (D_{2h})

Scheme 2 Schematic representation of initial geometries considered for optimization.

stable than the corresponding triplet state by 3.5 kcal mol^{-1}. Since the singlet state is more stable than the triplet state, we analyzed the geometries and bonding of the singlet states in detail.

A1–A4 show interesting structural variations depending on the carbones. **A1** and **A3** show a quasi-linear/linear C–B–B–C skeleton in which the carbone ligands are almost orthogonal (Table 1). The B1–B2 bond length in **A1** (1.512 Å) is longer than the corresponding triple bond length reported in diboryynes, whereas the said bond in **A3** is closer to a triple bond (1.487 Å). At the same time, the B–C bond length in **A1** (1.482 Å) is shorter than the corresponding single bond lengths, and the corresponding B–C bond length in **A3** (1.523 Å) is closer to the single-bond length.[7,11] One of the CO groups of the carbone ligand is bent in **A1**, whereas the other one is coordinated linearly. The $C–C_{CO(bent)}$ bond length is longer (1.449 Å) compared to that of the $C–C_{CO(linear)}$ bond (1.349 Å), and both bonds are longer than the $C–C_{CO}$ bond length in free $C(CO)_2$ (1.280 Å). Conversely, the C–P bond length (1.710 Å) in **A3** is significantly elongated compared to that in the free $C(PMe_3)_2$ group (1.639 Å). In addition, two of the $P–C_{Me}$ bonds are slightly shorter in boron-coordinated carbones than in non-coordinated carbones.

On the other hand, both **A2** and **A4** has a bent C–B–B–C skeleton (∠CBBC = 143° and 160°, respectively) with geometry in between that of H_2O_2 and *trans*-bent Si_2H_2. The B1–B2 bond length is closer to that of the triple bond in **A2** (1.483 Å) and **A4** (1.475 Å). However, the B–C bond lengths are in the range of those of single bonds (1.546 and 1.540 Å). The $C–C_{NHC}$ bond lengths (1.390 and 1.410 Å) are slightly longer in **A2** than the respective $C–C_{NHC}$ bond lengths in $C(NHC)_2$ (1.362 Å). In addition, the C–N bond lengths and C–C–N bond angles in **A2** are reduced compared to those of the non-coordinated carbones. The same scenario is present in **A4**. The $C–C_{cAAC}$ bond lengths (1.417 and 1.404 Å) are longer than those of the carbones (1.321 Å). Similarly, the C–N bond lengths are reduced in comparison with those of $C(cAAC)_2$.

MO analysis. The MOs of **A1–A4** were analyzed for both linear and bent geometries. The HOMO–LUMO gaps of the neutral systems are found to be in the range of 1.70–2.58 eV, which indicates their kinetic stability (Table S1†). The HOMOs are degenerate π MOs with a maximum coefficient on boron atoms in **A3** (Fig. 2a). These MOs exhibit major bonding interactions between the boron p orbitals with a slight antibonding interaction with carbon p orbitals corresponding to B–B π bonds. HOMO-1s are also degenerate MOs corresponding to the π-type lone pair on the carbone carbon atom. However, it is noteworthy that these lone-pair orbitals overlap with B π-type orbitals and P–C σ* orbitals, where the interaction with the former is significantly greater. The lone-pair orbital on the carbone carbon atom has significant back donation to the π* orbitals of CO, cAAC, and NHC as compared to the P–C σ* orbital of PMe_3. Accordingly, the π MOs of **A1**, **A2** and **A4** are quite different from that of **A3**. Since CO is an excellent π-acceptor with two sets of π MOs, the π* MOs are energetically low in $C(CO)_2$. Therefore, the carbone π-type lone-pair orbital and the B–B π orbital can overlap with the CO π* orbitals. The resulting orbitals are given in Fig. 2b. Note that NHC and cAAC have one set of π MOs as compared to the two orthogonal sets in CO. For that reason, to obtain an adequate overlap between the C–N π* MOs of two ligands attached to carbone and the B–B π MO and π-type lone pair on the carbone carbon atom, the C–B–B–C skeleton in **A2** and **A4** undergoes bending, resulting in geometry that is in between that of *trans*-Si_2H_2 and H_2O_2 (Fig. 1, 2c, d and Fig. S2†).

The above-discussed MOs can be considered as being generated by the interaction of the B_2 fragment with two CL_2 fragments. The ground state of B_2 is $^3\Sigma_g^-$ with the electronic configuration $1\sigma_g^2 1\sigma_u^2 1\pi_u^1 1\pi'^1_u$ (Scheme 1a). To form two B–C bonds by the donation of σ lone pairs on carbones to B_2, the two electrons from $1\sigma_u$ should be excited to $1\pi_u$ and $1\pi'_u$ (Scheme 3a). This excitation results in two vacant σ-type orbitals on B_2, which has the appropriate symmetry to interact with the linear combination of the σ-type carbone lone-pair orbitals. The in-phase combination of the carbone σ-type lone pairs has the correct symmetry to interact with the $2\sigma_g$ MO of B_2. On the other hand, the out-of-phase combination of the carbone σ-type lone pairs overlap with the $1\sigma_u$ MO of B_2. Consequently, the $1\sigma_g$, $1\pi_u$, and $1\pi'_u$ orbitals centered on B_2 are doubly occupied, resulting in a formal B–B triple bond character (Fig. S3†).

Table 1 Important bond lengths and bond angles in **A1–A4** and **B1–B4**

	Bond lengths (Å)		Bond angle (°)
	B–B	B–C	∠BBC
A1/B1	1.512/1.530	1.482/1.488	174.6/180.0
A2/B2	1.484/1.513	1.546/1.478	154.9/180.0
A3/B3	1.487/1.528	1.527/1.464	180.0/180.0
A4/B4	1.475/1.526	1.570/1.496	161.7/180.0

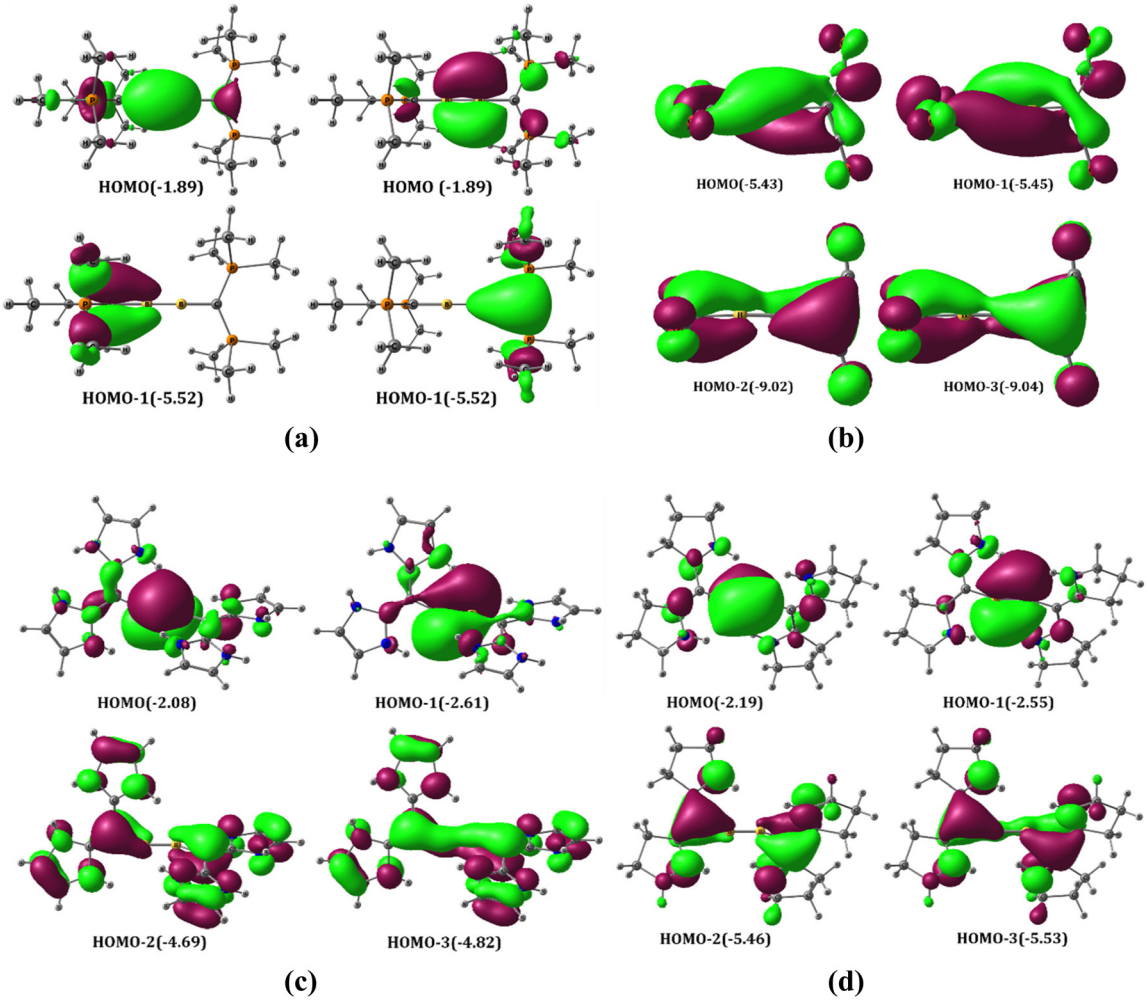

Fig. 2 Selected frontier π MOs of **A1–A4** (**A3** (a), **A1** (b), **A2** (c) and **A4** (d)) at the M06/def2-TZVPP//BP86/def2-TZVPP level of theory. Eigenvalues are given in eV in parentheses. The isosurface value is 0.03.

It is essential to point out that the MO analysis suggests the bonding picture in the **A1–A4** structures resembles the bonding scenario of a bisallylic anionic system (Fig. S4†). The HOMO and HOMO−3 constitute one allylic anionic system, and HOMO−1 and HOMO−2 constitute another orthogonal allylic anionic system for **A1**, **A2** and **A4**, but for **A3**, one HOMO and one HOMO−1 in similar planes make up the allylic anionic MO skeleton. However, the higher electronegativity of the carbon compared to that of the boron enforces the lone pairs to be more localized on carbone carbon atoms.

NBO/NPA analysis. The above-discussed bonding pattern from MO analysis is well corroborated with the numerical values obtained from the NBO analysis (Table 2). The NBO charge analysis indicates that $C(CO)_2$ is a net charge acceptor compared to other carbones, indicating that $C(CO)_2$ is a relatively better π acceptor than the σ donor. The other carbones are better σ donors than the π acceptor with decreasing order: $C(NHC)_2$ > $C(cAAC)_2$ > $C(PMe_3)_2$. The Wiberg bond indices (WBIs) for the B–B bond reveal its triple bond nature for **A2**, **A3** and **A4**, with values of 2.41, 2.19, and 2.42, respectively (Table 2). The lower value of the WBI for **A1** (1.49) is due to the significant delocalization of the electrons from the B–B π MOs to the CO π* orbitals, which is evident from the π MOs of **A1** (Fig. 2a). The occupancy data also show a significant deviation of electron density from the B1–B2 π-bonding MOs (1.15*e* and 1.02*e*) to the CO π* orbitals (2.4*e*) for **A1**. At the same time, the WBIs of B–C bonds for all the **A1–A4** compounds fall within the range of single bonds with values of 0.98 (**A1**), 0.91 (**A2**), 0.92 (**A3**) and 0.94 (**A4**).

To understand the effect of carbone coordination on the strength of the B–B bond, we calculated the bond dissociation energy (BDE) of the B–B bond in B_2 and **A1–A4** at the M06/def2-TZVPP//BP86/def2-TZVPP level of theory (reaction (R1), Table 3). The boron atom and BCL_2 fragments are in a doublet ground state. The calculated bond dissociation energy of the neutral B_2 molecule ($^3\Sigma_g^-$) is 58.9 kcal mol^{-1}, and the corresponding BDE values in **A1–A4** are very high (87–119 kcal mol^{-1}). The BDE follows the order **A2** (118.9 kcal mol^{-1}) > **A4** (105 kcal mol^{-1}) > **A3** (94 kcal mol^{-1}) > **A1** (87 kcal mol^{-1}). The

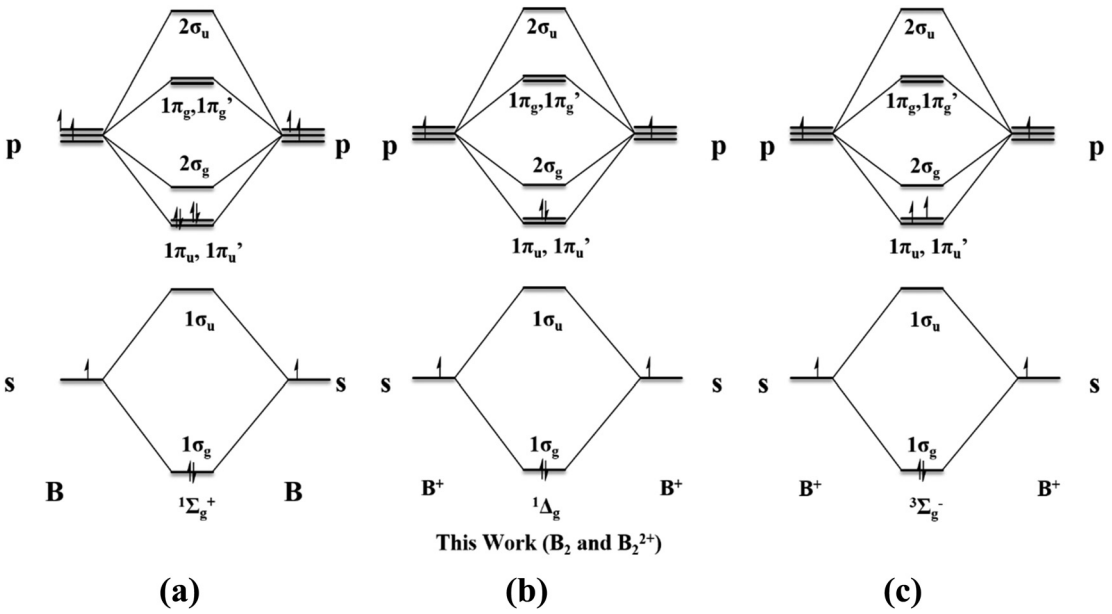

Scheme 3 MO diagram of the various excited states of B_2 and B_2^{2+} present in the study.

Table 2 The charge (*q*), Wiberg bond indices of selected bonds (P) of **A1–A4** at the M06/def2-TZVPP//BP86/def2-TZVPP level of theory

	Charge (*q*) (e)			WBI (P)	
Compounds	C3/C4	B_2	CL_2	B–B	B–C
A1	−0.84	0.40	−0.20	1.49	0.98
A2	−0.53	−0.76	0.38	2.41	0.91
A3	−1.49	−0.58	0.29	2.19	0.92
A4	−0.48	−0.74	0.37	2.42	0.94

dissociation energy indicates that $C(NHC)_2$ is better at stabilizing B≡B than the other carbones. The BDE for the B–B bond in **A1–A4** is comparable to the other theoretically reported BDEs for B≡B in B_2X_2 (X = CO, N_2 and BO^-) at the BP86/TZ2P level of theory reported by Frenking *et al.*, which is in the range of 83–149 kcal mol^{-1}.[7] We also calculated the complexation energy ($\Delta E_{complex}$) of **A1–A4** from the B_2 and $2CL_2$ fragments (reaction (R2)). The complexation energy follows the order **A2** (−185 kcal mol^{-1}) > **A4** (−165 kcal mol^{-1}) > **A3** (−152 kcal mol^{-1}) > **A1** (−77 kcal mol^{-1}), indicating the same trend as that of the BDE of the B–B bond.

We calculated the intrinsic B–B and B–C bond strengths by subtracting the preparation energy of the respective fragments from the negative dissociation energy ($\Delta E_{int} = -D_e - \Delta E_{prep}$). The preparation energy (ΔE_{prep}) of the respective fragments is calculated by subtracting the energy of the ground state of the fragment from the energy of the fragment in the same electronic and geometric state as exists in the complex. The electronic state of the BCL_2 fragments is considered in the quartet state with three unpaired electrons, *viz.* one in the σ orbital and one each in the orthogonal π orbitals. The B–B triple bond is formed by the interaction of the above-mentioned BCL_2 fragments. The preparatory energies for these fragments from the respective ground geometric and electronic states of BCL_2 are 65.6–91.3 kcal mol^{-1}. The calculated intrinsic B–B bond strengths follow the order **A2** (−184 kcal mol^{-1}) > **A3** (−179 kcal mol^{-1}) > **A1** (−178 kcal mol^{-1}) > **A4** (−177 kcal mol^{-1}).

The B–C bond in **A1–A4** is considered as being formed by the interaction of the B_2 fragment in the $^1\Sigma_g^+$ state with the two singlet CL_2 fragments. The preparatory energies for these fragment formations are quite low. As expected, the B–C bond strength (−68.9 to −106.5 kcal mol^{-1}), which is formally

Table 3 The dissociation energy of the B–B bonds ($D_{e\,B-B}$), complexation energy of two carbones with the B_2 unit ($\Delta E_{complex}$), and calculated interaction energies (ΔE_{int}) and preparatory energies (ΔE_{prep}) of the B–B bond and B–C bond of **A1–A4** at the M06/def2-TZVPP//BP86/def2-TZVPP level of theory

			ΔE_{int} (kcal mol^{-1})		ΔE_{prep} (kcal mol^{-1})	
Compounds	$D_{e\,B-B}$ (kcal mol^{-1})	$\Delta E_{complex}$ (kcal mol^{-1})	B–B	B–C	B–B	B–C
A1	87.1	−77.1	−178.3	−68.9	91.3	30.0
A2	118.9	−185.4	−184.5	−104.8	65.6	12.1
A3	93.4	−152.6	−179.3	−86.7	86.0	10.4
A4	105.3	−165.1	−177.4	−106.5	72.1	23.9

a single bond, is much weaker than the formal B–B triple bond.

$$[(L_2C)\cdot B_2\cdot(CL_2)]^n \rightarrow 2BCL_2{}^{n/2}\ (n = 0/+2) \quad (R1)$$

$$[(L_2C)\cdot B_2\cdot(CL_2)]^n \rightarrow B_2{}^n + 2CL_2\ (n = 0/+2) \quad (R2)$$

QTAIM analysis . The topological analysis of the electron density of **A1–A4** was performed to obtain a detailed picture of the bonding. Important parameters at the bond critical points are listed in Table 4. The Laplacian for **A3** in the B1–B2–P7 plane is given in Fig. 3, and all others are given in the ESI (Fig. S5†). The Laplacian of electron densities at the bond critical points of the B–B bonds are very high negative values, whereas those at the B–C bonds are close to zero, indicating the covalent nature of the B–B bond and polar covalent coordinate nature of the B–C bond. The degree of covalence of the B–B bond and B–C bonds was calculated by using the expression $H(r)/\rho(r)$. Interestingly, the covalence of the B–C bond is comparatively higher than that of the B–B bond. The ellipticity at the BCP can be depicted as a measure of the anisotropy of the curvature of the electron density in the directions normal to the bond, and the magnitude of this ellipticity can give insights into the multiple bonding that present. Here, close to zero ε values at the BCP match the triple-bond character of the B–B bond shown by the MO and geometry analysis. **A1** and **A3** with their linear C–B–B–C skeleton show bond ellipticity of the B–C bond in the range of 0.22–0.25, indicating that the π delocalization in orthogonal planes is different. This is in agreement with the geometrical and MO data. On the other hand, **A2** and **A4** with their bent C–B–B–C skeleton show bond ellipticity of the B–C bond close to zero, which agrees with the frontier MOs showing more delocalized MOs in orthogonal planes (HOMO−2 and HOMO−3).

Structure and bonding analysis of the doubly carbone-coordinated diboron dication

We also studied carbone coordination with the diboron dication, which has a different electronic structure to that of the neutral system. We calculated the equilibrium geometries of singlet and triplet states for $[(L_2C)\cdot B_2\cdot(CL_2)]^{2+}$ (Fig. 4) by choosing D_{2d} and D_{2h} point group symmetric geometries as initial

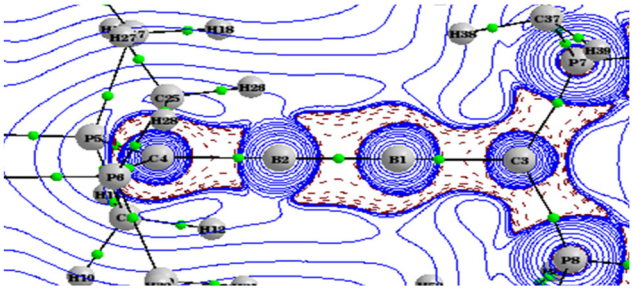

Fig. 3 The Laplacian of the electron density plotted in the plane of B1–B2–P7 of **A3**. BCPs are marked by green dots. The wave function was generated at the M06/def2-TZVPP//BP86/def2-TZVPP level of theory.

geometries (Scheme 2). **B1–B4** denote dicationic $[(L_2C)\cdot B_2\cdot(CL_2)]^{2+}$ compounds and **1–4** indicate the type of carbone coordinated to $B_2{}^{2+}$. The number 1 indicates that the carbone coordinated to $B_2{}^{2+}$ is $C(CO)_2$; similarly, numbers 2, 3 and 4 indicate that the type of carbone coordinated to $B_2{}^{2+}$ is $C(NHC)_2$, $C(PMe_3)_2$ and $C(cAAC)_2$ respectively. The T in parentheses indicates the triplet-state isomer of the molecule (Fig. 4, Fig. S6). Both planar cumulenic (D_{2h})/pseudo-planar cumulenic (D_2) and non-planar cumulenic D_{2d}/S_4 geometries were found to be stationary points on the potential energy surface. The singlet states converged into planar cumulenic/pseudo-planar cumulenic geometries, whereas the triplet states converged into non-planar cumulenic geometries. The ground states of **B2** and **B3** are singlet states with pseudo-planar cumulenic and planar cumulenic geometries, respectively. At the same time, **B1** and **B4** are in triplet states with non-planar cumulenic geometries. The relative energy difference between the singlet and triplet states reduces and follows the order PMe_3 (8.05) > NHC (5.49) > CO (−0.95) and cAAC (−3.53). Note that the energy differences between the singlet and triplet states of **B1** and **B4** are only marginal. Hence, we considered both singlet and triplet geometries of **B1** and **B4** for detailed study.

All the **B1–B4** possess a linear C–B–B–C skeleton. The B–B bond lengths in singlet cumulenic geometries are between the reported double and triple bond lengths (1.530–1.513 Å). On the other hand, the B–C bond lengths fall within the double

Table 4 Topological parameters of the electron density at the bond critical points of selected bonds of **A1–A4** calculated at the M06/def2-TZVPP//BP86/def2-TZVPP level of theory

Compounds	Bond	$\rho(r)^a$	$\nabla^2\rho(r)^b$	$V(r)^c$	$G(r)^d$	$H(r)^e$	ε^f	$H(r)/\rho(r)$
A1	B–B	0.1900	−0.4547	−0.2142	0.0502	−0.1640	0.0	−0.86
	B–C	0.1852	0.0252	−0.3952	0.2007	−0.1944	0.26	−1.05
A2	B–B	0.1761	−0.3206	−0.2229	0.0713	−0.1515	0.06	−0.86
	B–C	0.1741	−0.0291	−0.3530	0.1728	−0.1801	0.05	−1.03
A3	B–B	0.1779	−0.3306	−0.2196	0.0685	−0.1511	0.0	−0.85
	B–C	0.1674	0.0283	−0.3421	0.1746	−0.1675	0.22	−1.00
A4	B–B	0.1811	−0.3379	−0.2328	0.0741	−0.1586	0.0	−0.88
	B–C	0.1800	−0.0489	−0.3665	0.1771	−0.1893	0.06	−1.05

[a] Electron density ($\rho(r)$, e Bohr^{-3}). [b] Laplacian of electron density ($\nabla^2\rho(r)$, e Bohr^{-5}). [c] Potential energy density ($V(r)$, Hartree Bohr^{-3}). [d] Kinetic energy density ($G(r)$, Hartree Bohr^{-3}). [e] Total energy density ($H(r)$, Hartree Bohr^{-3}). [f] Ellipticity (ε). $H(r)/\rho(r)$ gives the degree of covalence.

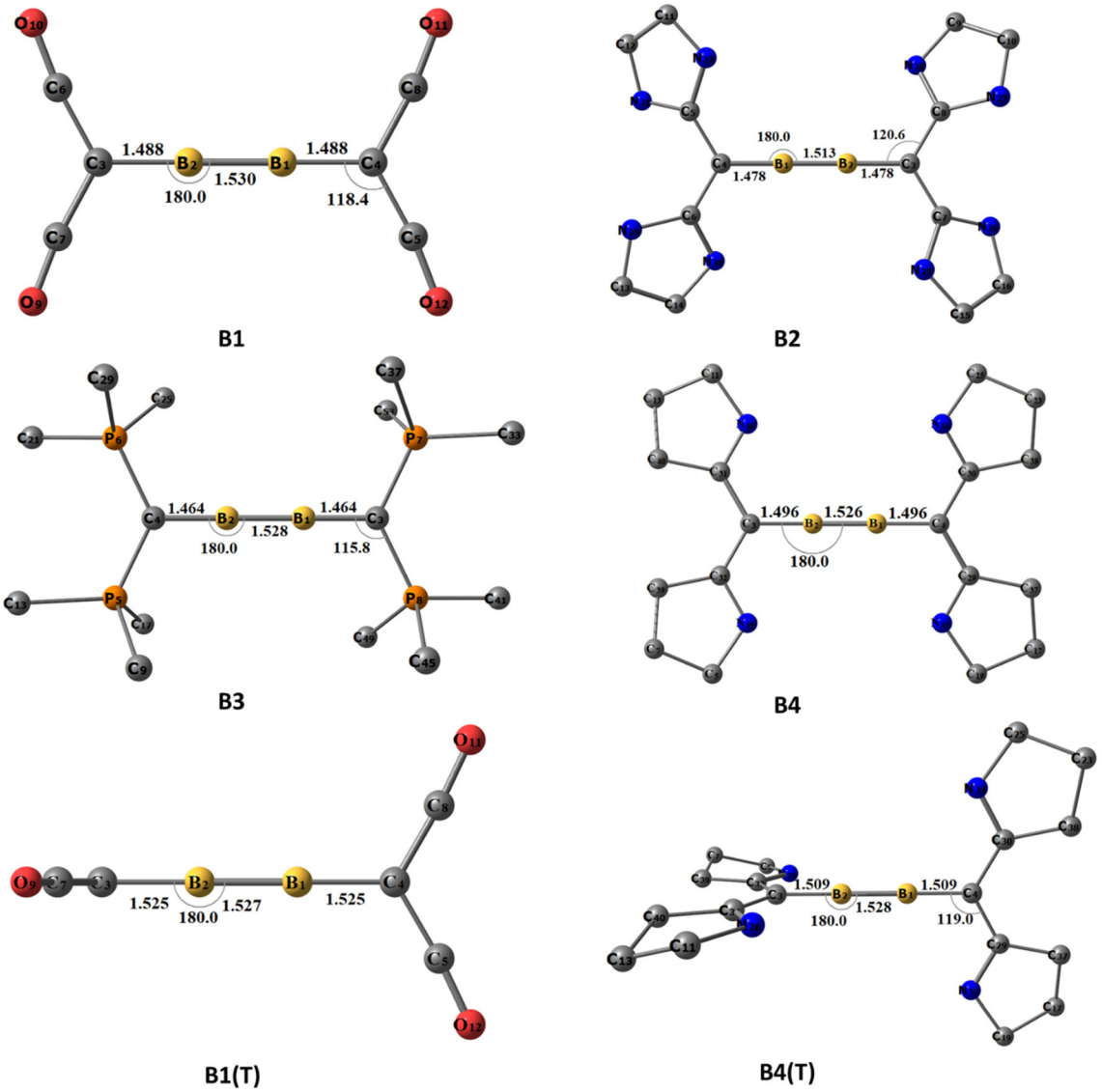

Fig. 4 The equilibrium geometries and the important structural parameters of **B1–B4**. For $[((CO)_2C)\cdot B_2\cdot(C(CO)_2)]^{2+}$ and $[((cAAC)_2C)\cdot B_2\cdot(C(cAAC)_2)]^{2+}$ both singlet and triplet geometries are given. T indicates a triplet state, and the rest are singlet states. Optimized at the BP86/def2-TZVPP level of theory. Distances are given in Ångstroms, and angles are given in degrees. Hydrogens are omitted for a better view.

bond length range (1.496–1.464 Å). There are no significant changes in the geometric parameters for triplet **B1(T)** and **B4 (T)** as compared to the respective singlet geometries (the B–B bond lengths are 1.527 and 1.528 Å, the B–C bond lengths are 1.525 and 1.509 Å for **B1** and **B4**, respectively). This can be attributed to the stronger π-accepting nature of CO and cAAC ligands, stabilizing both B–B π MOs through delocalization in orthogonal planes. In all **B1–B4**, the C–X_L (X_L = C/P) bond lengths are significantly elongated compared to those in their free carbone scenarios, which indicate the reduction of π back donation from the carbone carbon centre.

MO analysis. The MO analysis of planar/pseudo-planar cumulenic singlet **B1–B4** indicates that the frontier MOs are similar to the butatriene π MOs (Fig. 5a–d). The HOMO–LUMO gaps of the dicationic systems are found to be in the range of 2.56–2.98 eV, which indicate their kinetic stability (Table S1†). The HOMOs in all cases are localized to the B–B π MO. HOMO−1 and HOMO−2 are linear combinations of π MOs having zero and one node, respectively. The nature of these MOs is similar to typical π MOs of butadiene. These MOs can be considered as formed by the interaction of B_2^{2+} with carbone ligands. The ground state of B_2^{2+} is $^1\Sigma_g^+$ with the electronic configuration $1\sigma_g^2 1\sigma_u^2 1\pi_u^0 1\pi'^0_u 2\sigma_g^0 1\pi_g^0 1\pi'^0_g$ (Scheme 3). The excitation of two electrons from $1\sigma_u$ to one of the bonding π MOs results in the $^1\Delta_g$ state with the electronic configuration $1\sigma_g^2 1\sigma_u^0 1\pi_u^2 1\pi'^0_u 2\sigma_g^0 1\pi_g^0 1\pi'^0_g$. The bonding and antibonding combination of σ-type lone-pair orbitals on carbone carbons can donate to the $2\sigma_g$ and $1\sigma_u$ orbitals centered on B_2^{2+}, respectively, leading to two B–C σ bonds (Fig. S7†). Similarly, the bonding and antibonding combi-

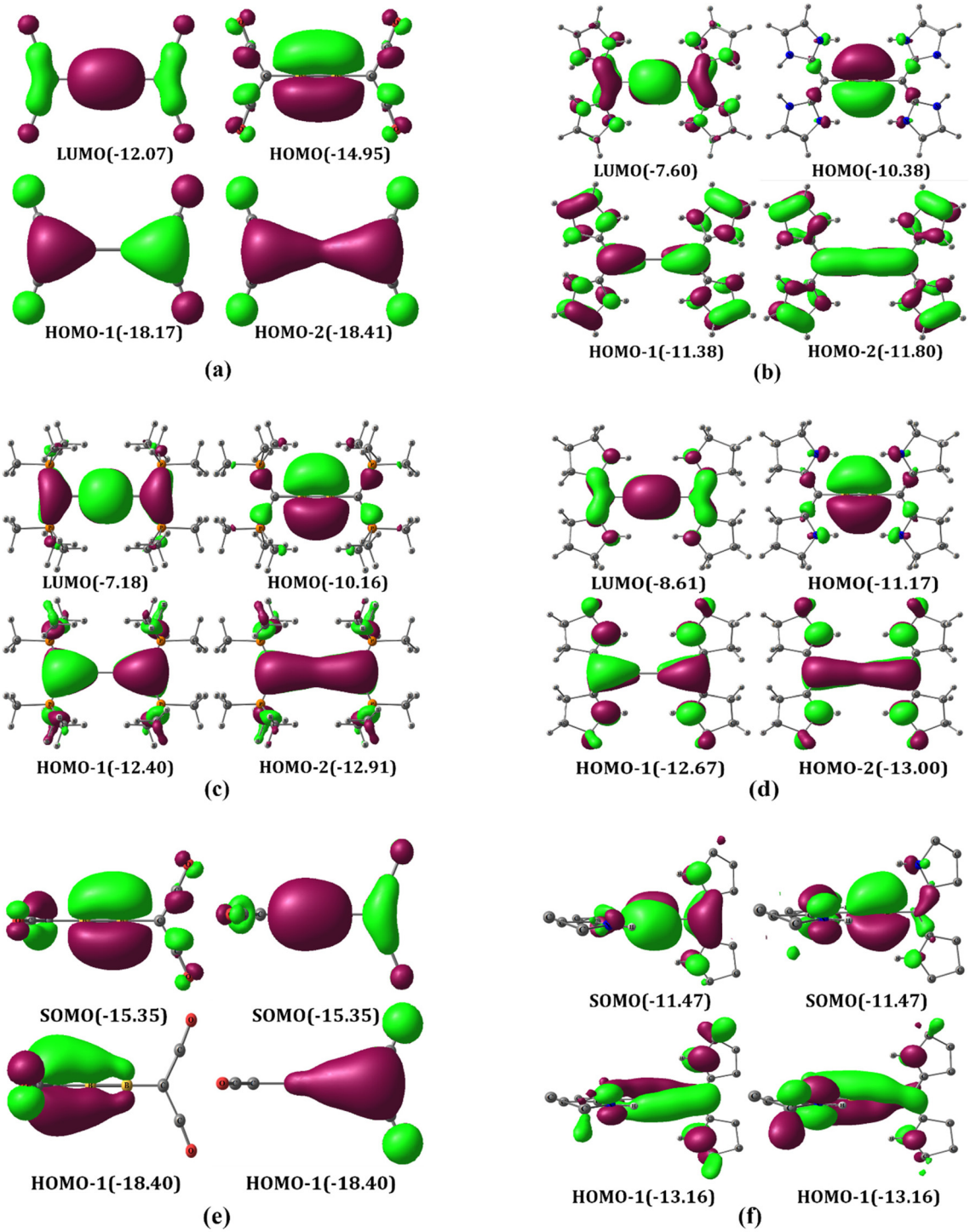

Fig. 5 Selected frontier π MOs of **B1** (singlet) (a), **B2** (b), **B3** (c), **B4** (singlet) (d), **B1(T)** (e) and **B4(T)** (f) at the M06/def2-TZVPP//BP86/def2-TZVPP level of theory. For triplet states, low-lying alpha orbitals are given. Eigenvalues are given in eV in parentheses. The isosurface value is 0.03.

nations of π-type lone-pair orbitals on carbone carbons can donate to the $1\pi'_u$ and $1\pi'_g$ orbitals of the B_2^{2+} moiety, resulting in two delocalized π MOs (HOMO−1 and HOMO−2, Fig. 5a–d). Accordingly, each carbone acts as a four-electron donor to B_2^{2+}, resulting in a diborabutatriene system. The butadiene-type π MOs are highly stabilized when the carbone is $C(CO)_2$ followed by $C(cAAC)_2$, $C(PMe_3)_2$, and $C(NHC)_2$. These energetic orders were followed based on the π-accepting strength of ligands (L) as well as the possibility of more delocalization.

The triplet non-planar **B1(T)** has two sets of orthogonal allylic π MOs and resembles a bisallylic radical system. The all-

in-phase combination of degenerate π MOs are doubly occupied (HOMO−1). The degenerate π MOs with one node passing through the B–C bond are singly occupied (SOMO). The π MOs of **B4** are almost similar to those of **B1** except for all in-phase combinations, which are delocalized through four atoms similar to that of Mobius π delocalization (Fig. 5e and f). These π MOs can be interpreted as being formed by the interaction of B_2^{2+} in the $^3\Sigma_g^-$ state ($1\sigma_u^0 1\pi_u^1$, $1\pi'^1_u$) with π-type lone pairs on the carbone carbon *viz.* the bonding combination results in degenerate HOMO−1 while the antibonding combination results in degenerate SOMO.

NBO/NPA analysis. The above-mentioned MO description is correlated well with the localized bonding description obtained from the NBO analysis (Table 5). The Wiberg bond indices are higher for the B–B bond than they are for the B–C bond, indicating the non-polar double-bond nature of the former bond. Since CO and cAAC are better π acceptors than NHC and PMe_3, the WBIs of the B–C bond of **B1** and **B4** have relatively low values. These WBI values correlate well with the diborabutatriene bonding description obtained from the MO analysis for the singlet cumulenic geometries. Note that the WBI of the B–B bond in **B1–B4** is lower than that in **A1–A4**, indicating a delocalized B–B double-bond nature for the former and a triple bond for the latter. The charge decomposition analysis also suggests that $C(NHC)_2$ (0.89*e*) and $C(PMe_3)_2$ (0.83*e*) are relatively better donors towards B_2^{2+} as compared with $C(CO)_2$ (0.60*e*) and $C(cAAC)_2$ (0.81*e*).

Table 5 The charge (*q*) and Wiberg bond indices of selected bonds (P) of **B1–B4** at the M06/def2-TZVPP//BP86/def2-TZVPP level of theory. T in parentheses denotes triplet minima, and the rest are singlet minima

	Charge (*q*) (*e*)			WBI (P)	
Compounds	C3/C4	B_2	CL_2	B–B	B–C
B1	−0.87	0.80	0.60	1.73	1.01
B2	−0.63	0.21	0.89	1.89	1.20
B3	−1.42	0.34	0.83	1.80	1.28
B4	−0.64	0.38	0.81	1.86	1.12
B1(T)	−0.86	0.84	0.58	1.40	0.90
B4(T)	−0.64	0.51	0.75	1.81	1.03

We further calculated the bond dissociation energy of the B–B bond by fragmenting the molecule into two $[B(CL_2)]^+$ groups (reaction (R1)). The ground state of the $[BCL_2]^+$ fragment is singlet with one lone pair of electrons on the boron atom and an empty p-orbital, similar to that of singlet carbene. The calculated bond dissociation energy (37.8–69.9 kcal mol^{-1}) is lower than that of the corresponding neutral system (Table 6). However, the BDE values of **B2** and **B4** are higher than those of **B1** and **B3**. We also calculated the complexation energy for the formation of **B1–B4** from the B_2^{2+} (triplet state) and $(CL_2)_2$ (singlet) fragments (reaction (R2)). The corresponding complexation energy is found to be much more exothermic compared to that of neutral systems. Even though the B–C bond in a dicationic system is much stronger than that of the B–C bond in a neutral system, as evident from geometrical and NBO analysis, this much higher negative complexation energy can be attributed to the instability of B_2^{2+} as compared to the neutral B_2.

We also calculated the intrinsic B–B and B–C bond strengths. The B–B bonds are considered as being formed by the interaction of two BCL_2^+ fragments in the triplet state, *viz.* one electron in a σ orbital and one electron in a π orbital. Since the B–B bond is formally a double bond, the calculated intrinsic bond strength is found to be much smaller than that in **A1–A4**. The B–C bond is formed by the interaction of the B_2 fragment in the $^1\Delta_g$ and $^3\Sigma_g^-$ states (for the singlet and triplet states, respectively) with the two singlet CL_2 fragments. Note that the intrinsic bond strength is found to be higher than that in **A1–A4**, indicating a formal B–C double-bond nature.

QTAIM analysis. Topological analysis of the electron density of **B1–B4** was carried out to acquire more details on the bonding nature using the QTAIM method (Table 7). The Laplacian of electron density in the molecular plane for **B3** and **B4(T)** are given in Fig. 6. The corresponding plots for other molecules are given in the ESI.† The electron density and the Laplacian of electron density at the BCP of B–B and B–C have higher values as compared to those in the neutral system. We wish to point out that the electron density cannot be correlated to the strength of the bond.[41] Nevertheless, the covalence of the B–B bond in the dicationic system is similar to that of the neutral system, whereas the covalence of the B–C bond in the dicationic system is slightly higher. The ellipticity

Table 6 The dissociation energy of the B−B bonds ($D_{e\,B-B}$) and complexation energy of two carbones with the B_2^{2+} unit ($\Delta E_{complex}$), and calculated interaction energies (ΔE_{int}) and preparatory energies (ΔE_{prep}) of the B−B bond and B−C bond of **B1–B4** at the M06/def2-TZVPP//BP86/def2-TZVPP level of theory. T in parentheses denotes triplet minima, and the rest are singlet minima

			ΔE_{int} (kcal mol^{-1})		ΔE_{prep} (kcal mol^{-1})	
Compounds	$D_{e\,B-B}$ (kcal mol^{-1})	$\Delta E_{complex}$ (kcal mol^{-1})	B–B	B–C	B–B	B–C
B1	37.8	−311.9	−83.8	−207.2	46.0	51.3
B2	69.9	−578.7	−122.0	−335.3	52.1	46.0
B3	57.1	−564.1	−122.1	−326.3	65.0	44.3
B4	64.4	−532.5	−116.6	−326.8	52.2	60.5
B1(T)	38.8	−312.8	−84.8	−196.7	46.0	40.2
B4(T)	67.9	−536.0	−120.2	−326.8	52.3	58.8

Table 7 Topological parameters of the electron density at the bond critical points of selected bonds of **B1–B4** calculated at the M06/def2-TZVPP//BP86/def2-TZVPP level of theory

Compound	Bond	$\rho(r)^a$	$\nabla^2\rho(r)^b$	$V(r)^c$	$G(r)^d$	$H(r)^e$	ε^f	$H(r)/\rho(r)$
B1	B–B	0.1922	−0.4816	−0.2108	0.0452	−0.1656	0.69	−0.86
	B–C	0.1938	−0.0629	−0.4079	0.1961	−0.2118	0.22	−1.09
B2	B–B	0.1905	−0.4594	−0.2165	0.0508	−0.1657	0.59	−0.87
	B–C	0.2036	−0.0813	−0.4305	0.2051	−0.2254	0.05	−1.10
B3	B–B	0.1880	−0.4553	−0.2073	0.0467	−0.1606	0.57	−0.85
	B–C	0.2013	−0.0500	−0.4280	0.2077	−0.2203	0.07	−1.09
B4	B–B	0.1904	−0.4694	−0.2120	0.0473	−0.1647	0.63	−0.86
	B–C	0.2053	−0.1992	−0.4161	0.1831	−0.2330	0.10	−1.13
B1(T)	B–B	0.1880	−0.4322	−0.2102	0.0511	−0.1591	0.0	−0.85
	B–C	0.1847	−0.1432	−0.3705	0.1673	−0.2032	0.02	−1.10
B4(T)	B–B	0.1864	−0.4245	−0.2087	0.0513	−0.1574	0.0	−0.84
	B–C	0.2054	−0.2819	−0.4032	0.1664	−0.2369	0.07	−1.15

[a] Electron density ($\rho(r)$, e Bohr^{-3}). [b] Laplacian of electron density ($\nabla^2\rho(r)$, e Bohr^{-5}). [c] Potential energy density ($V(r)$, Hartree Bohr^{-3}). [d] Kinetic energy density ($G(r)$, Hartree Bohr^{-3}). [e] Total energy density ($H(r)$, Hartree Bohr^{-3}). [f] Ellipticity (ε). T in parentheses indicates triplet minima and the rest are singlet minima.

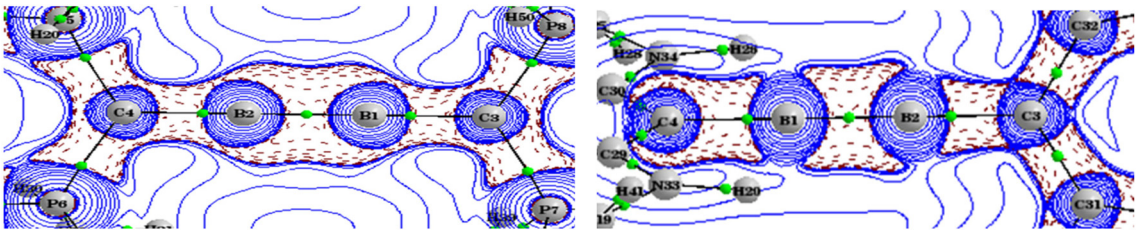

(a) (b)

Fig. 6 The Laplacian of the electron density plotted in the plane of B1–B2–P7 of **B3** (a) and in the plane of B1–B2–C32 of **B4(T)** (b). BCPs are marked by green dots. The wave function was generated at the M06/def2-TZVPP//BP86/def2-TZVPP level of theory.

(ε) values of the B–B bond in singlet cumulenic systems show significant magnitudes (0.57–0.69), which substantiate the diborabutatriene skeleton shown by MO and NBO analysis. At the same time, the triplet **B1** and **B4** have almost zero ε values correlating with the degenerate orthogonal half-filled π orbitals.

Conclusions

We carried out the computational study of carbone-coordinated diborons in their neutral ($[(L_2C)\cdot B_2\cdot(CL_2)]$) and dicationic ($[(L_2C)\cdot B_2\cdot(CL_2)]^{2+}$) states, where L = CO, NHC, PMe_3 and cAAC. The structure and bonding analysis show that the $[(L_2C)\cdot B_2\cdot(CL_2)]$ possesses a singlet non-planar cumulenic ground state independent of the ligands attached to the carbone carbon. The MO analysis depicted an orthogonal bisallylic anion-type system constituted by the two orthogonal B–B π bonds and the carbone π lone pairs, where the carbone π lone pairs are more localized on the carbons. The MOs suggest that the B_2 fragment is in a $^1\Sigma_g^+$ excited state and interacts with the two CL_2 fragments. NBO and QTAIM analyses confirm that the singlet non-planar cumulenic geometry exhibits a triple bond between the borons, reminiscent of the diborabutyne system. The bond dissociation energy and interaction energy indicate that carbone coordination strengthens the B–B bond and is comparable with the reported diboron complexes. On the other hand, the dicationic $[(L_2C)\cdot B_2\cdot(CL_2)]^{2+}$ displays singlet planar cumulenic/pseudo-planar cumulenic and triplet non-planar cumulenic minima. Singlet cumulenic states are found to be the ground state when the carbone is $C(NHC)_2$ and $C(PMe_3)_2$, whereas for carbones $C(CO)_2$ and $C(cAAC)_2$, the triplet minima are found to be more stable. Even though the singlet–triplet energy difference is minimal, this variation can be attributed to the more π-accepting nature of CO and cAAC. The MO analysis indicates that in singlet cumulenic states, the C–B–B–C skeleton is similar to that of butatriene, *viz.* one localized B–B π MO, and two delocalized C–B–B–C π MOs. The NBO and QTAIM analyses support the MO picture, revealing the dual donation of CL_2 to the excited $^1\Delta_g$ B_2^{2+} state. In the case of triplet non-planar cumulenic states, the C–B–B–C π MOs suggest a bisallylic radical-type bonding, where the carbone lone pairs are more localized on the carbons due to its higher electronegativity. The bond dissociation and interaction energies show a weaker B–B bond and stronger B–C bonds than those in the neutral analogue. This work envisages that using double donor ligands such as carbones can stabilize the diboron moiety effectively, and the

careful tuning of electronic factors can alter the bonding and structure of the molecule.

Computational methodology

All calculations were carried out using the Gaussian09 programming package.[42] Geometry optimizations were performed at the DFT level using the exchange functional of Becke in conjunction with the correlation functional of Perdew (BP86).[43–45] The basis set used was a triple zeta valence with double polarisation (def2-TZVPP), which can be notated as BP86/def2-TZVPP.[46] The analytical frequencies were calculated using the Hessian matrix to confirm the minima. Single-point calculations were carried out at the M06/def2-TZVPP level of theory.[47] Various recent studies from our group have found that the GGA functional reproduces the experimental geometries very well, whereas the meta-GGA functional gives more accurate energetics and molecular properties. The electronic energy from the M06/def2-TZVPP level of theory was added with the zero point correction from the optimization at the BP86/def2-TZVPP level of theory. Zero point correction gives the molecular energy in the lowest vibrational levels at absolute zero (0 K). The corrected energies were used to calculate the bond dissociation energies (D_e), interaction energies (ΔE_{int}), and preparatory energies (ΔE_{prep}). Natural bond orbital and natural population analyses were performed at the M06/def2-TZVPP//BP86/def2-TZVPP level of theory using the NBO 6.0 package.[48] The electronic topological analysis was conducted using the quantum theory of atoms in molecules (QTAIM) methodology in the AIMALL package.[49–51] The wave function input for QTAIM analysis was generated using the Gaussian09 program package at the M06/def2-TZVPP//BP86/def2-TZVPP level of theory.

Conflicts of interest

There are no conflicts to declare.

Acknowledgements

PP thanks SERB, India, for the financial support. JS thanks UGC, India for providing the fellowship. PP and JS also thank the Centre for Computational Modelling and Simulation (CCMS) and Central Computer Center (CCC) at NITC for the computational facilities.

References

1 H. Li, G. Xu, S. Li, Y. Wu and Z. Lu, *Chem. Rec.*, 2023, **23**, e202300238.
2 Y. F. Lin and C. W. Chiu, *Chem. Lett.*, 2017, **46**, 913–922.
3 S. Tam, M. Macler, M. E. DeRose and M. E. Fajardo, *J. Chem. Phys.*, 2000, **113**, 9067–9078.
4 M. Zhou, N. Tsumori, Z. Li, K. Fan, L. Andrews and Q. Xu, *J. Am. Chem. Soc.*, 2002, **124**, 12936–12937.
5 A. Papakondylis, E. Miliordos and A. Mavridis, *J. Phys. Chem. A*, 2004, **108**, 4335–4340.
6 S. D. Li, H. J. Zhai and L. S. Wang, *J. Am. Chem. Soc.*, 2008, **130**, 2573–2579.
7 L. C. Ducati, N. Takagi and G. Frenking, *J. Phys. Chem. A*, 2009, **113**, 11693–11698.
8 H. Braunschweig, R. D. Dewhurst, K. Hammond, J. Mies, K. Radacki and A. Vargas, *Science*, 2012, **336**, 1420–1422.
9 G. Frenking and N. Holzmann, *Science*, 2012, **336**, 1394–1395.
10 N. Holzmann, M. Hermann and G. Frenking, *Chem. Sci.*, 2015, **6**, 4089–4094.
11 Y. Wang, B. Quillian, P. Wei, C. S. Wannere, Y. Xie, R. B. King, H. F. Schaefer, P. V. R. Schleyer and G. H. Robinson, *J. Am. Chem. Soc.*, 2007, **129**, 12412–12413.
12 J. Böhnke, H. Braunschweig, W. C. Ewing, C. Hörl, T. Kramer, I. Krummenacher, J. Mies and A. Vargas, *Angew. Chem., Int. Ed.*, 2014, **53**, 9082–9085.
13 M. Soleilhavoup and G. Bertrand, *Acc. Chem. Res.*, 2015, **48**, 256–266.
14 V. Nesterov, D. Reiter, P. Bag, P. Frisch, R. Holzner, A. Porzelt and S. Inoue, *Chem. Rev.*, 2018, **118**, 9678–9842.
15 W. Lu, Y. Li and R. Kinjo, *J. Am. Chem. Soc.*, 2019, **141**, 5164–5168.
16 W. Lu, Y. Li, R. Ganguly and R. Kinjo, *Angew. Chem., Int. Ed.*, 2017, **56**, 9829–9832.
17 J. Böhnke, M. Arrowsmith and H. Braunschweig, *J. Am. Chem. Soc.*, 2018, **140**, 10368–10373.
18 O. Ciobanu, E. Kaifer, M. Enders and H. J. Himmel, *Angew. Chem., Int. Ed.*, 2009, **48**, 5538–5541.
19 J. Fan, A.-P. Koh, J. Zhou, Z.-F. Zhang, C.-S. Wu, R. D. Webster, M.-D. Su and C.-W. So, *J. Am. Chem. Soc.*, 2023, **145**, 11669–11677.
20 D. E. Trujillo-González, G. González-García, T. A. Hamlin, F. M. Bickelhaupt, H. Braunschweig, J. O. C. Jiménez-Halla and M. Solà, *Eur. J. Inorg. Chem.*, 2023, e202200767.
21 R. Saha, S. Pan and P. K. Chattaraj, *ACS Omega*, 2018, **3**, 13720–13730.
22 R. Tonner and G. Frenking, *Chem. – Eur. J.*, 2008, **14**, 3260–3272.
23 G. Frenking and R. Tonner, *Pure Appl. Chem.*, 2009, **81**, 597–614.
24 G. Frenking, R. Tonner, S. Klein, N. Takagi, T. Shimizu, A. Krapp, K. K. Pandey and P. Parameswaran, *Chem. Soc. Rev.*, 2014, **43**, 5106–5139.
25 A. L. Liberman-Martin, *Cell Rep. Phys. Sci.*, 2023, **4**, 101519.
26 F. Ramirez, N. B. Desai, B. Hansen and N. McKelvie, *J. Am. Chem. Soc.*, 1961, **83**, 3539–3540.
27 R. Tonner and G. Frenking, *Angew. Chem., Int. Ed.*, 2007, **46**, 8695–8698.
28 G. Frenking and R. Tonner, *Wiley Interdiscip. Rev.: Comput. Mol. Sci.*, 2011, **1**, 869–878.
29 C. A. Dyker, V. Lavallo, B. Donnadieu and G. Bertrand, *Angew. Chem., Int. Ed.*, 2008, **47**, 3206–3209.

30 A. Fürstner, M. Alcarazo, R. Goddard and C. W. Lehmann, *Angew. Chem.*, 2008, **120**, 3254–3258.
31 L. Zhao, C. Chai, W. Petz and G. Frenking, *Molecules*, 2020, **25**, 4943.
32 C. Pranckevicius, L. Fan and D. W. Stephan, *J. Am. Chem. Soc.*, 2015, **137**, 5582–5589.
33 Y.-C. Hsu, J.-S. Shen, B.-C. Lin, W.-C. Chen, Y.-T. Chan, W.-M. Ching, G. P. A. Yap, C.-P. Hsu and T.-G. Ong, *Angew. Chem., Int. Ed.*, 2015, **54**, 2420–2424.
34 C. C. Roberts, D. M. Matías, M. J. Goldfogel and S. J. Meek, *J. Am. Chem. Soc.*, 2015, **137**, 6488–6491.
35 M. J. Goldfogel, C. C. Roberts and S. J. Meek, *J. Am. Chem. Soc.*, 2014, **136**, 6227–6230.
36 B. Inés, M. Patil, J. Carreras, R. Goddard, W. Thiel and M. Alcarazo, *Angew. Chem., Int. Ed.*, 2011, **50**, 8400–8403.
37 W. Petz, F. Öxler, B. Neumüller, R. Tonner and G. Frenking, *Eur. J. Inorg. Chem.*, 2009, 4507–4517.
38 M. Hermann and G. Frenking, *Chem. – Eur. J.*, 2017, **23**, 3347–3356.
39 N. Holzmann, A. Stasch, C. Jones and G. Frenking, *Chem. – Eur. J.*, 2011, **17**, 13517–13525.
40 N. Đorđević, R. Ganguly, M. Petković and D. Vidović, *Chem. Commun.*, 2016, **52**, 9789–9792.
41 L. Zhao, S. Pan and G. Frenking, *J. Chem. Phys.*, 2022, **157**, 034105.
42 M. J. Frisch, G. W. Trucks, H. B. Schlegel, G. E. Scuseria, M. A. Robb, J. R. Cheeseman, G. Scalmani, V. Barone, B. Mennucci, G. A. Petersson, H. Nakatsuji, M. Caricato, X. Li, H. P. Hratchian, A. F. Izmaylov, J. Bloino, G. Zheng, J. L. Sonnenberg, M. Hada, M. Ehara, K. Toyota, R. Fukuda, J. Hasegawa, M. Ishida, T. Nakajima, Y. Honda, O. Kitao, H. Nakai, T. Vreven, Jr., J. A. Montgomery, J. E. Peralta, F. Ogliaro, M. Bearpark, J. J. Heyd, E. Brothers, K. N. Kudin, V. N. Staroverov, R. Kobayashi, J. Normand, K. Raghavachari, A. Rendell, J. C. Burant, S. S. Iyengar, J. Tomasi, M. Cossi, N. Rega, J. M. Millam, M. Klene, J. E. Knox, J. B. Cross, V. Bakken, C. Adamo, J. Jaramillo, R. Gomperts, R. E. Stratmann, O. Yazyev, A. J. Austin, R. Cammi, C. Pomelli, J. W. Ochterski, R. L. Martin, K. Morokuma, V. G. Zakrzewski, G. A. Voth, P. Salvador, J. J. Dannenberg, S. Dapprich, A. D. Daniels, Ö. Farkas, J. B. Foresman, J. V. Ortiz, J. Cioslowski and D. J. Fox, *Gaussian 09 Revision E.01*, Gaussian Inc., Wallingford, CT, 2016.
43 A. D. Becke, *Phys. Rev. A: At., Mol., Opt. Phys.*, 1988, **38**, 3098–3100.
44 J. P. Perdew, *Phys. Rev. B: Condens. Matter Mater. Phys.*, 1986, **33**, 8822–8824.
45 J. P. Perdew, *Phys. Rev. B: Condens. Matter Mater. Phys.*, 1986, **34**, 7406–7406.
46 F. Weigend and R. Ahlrichs, *Phys. Chem. Chem. Phys.*, 2005, **7**, 3297.
47 Y. Zhao and D. G. Truhlar, *Theor. Chem. Acc.*, 2008, **120**, 215–241.
48 E. D. Glendening, C. R. Landis and F. Weinhold, *J. Comput. Chem.*, 2013, **34**, 1429–1437.
49 R. F. W. Bader and R. F. Bader, *Atoms in Molecules: A Quantum Theory*, Clarendon Press, 1990.
50 *The Quantum Theory of Atoms in Molecules*, ed. C. F. Matta and R. J. Boyd, Wiley, 2007.
51 T. A. Keith, *TK Gristmill Software*, Overland Park KS, USA, 2015.